

Supplementary Data

Petrography and previous geochemical analyses

For stratigraphic ages of samples (from stage to ammonite zones) within the sedimentary formations, correlations between wells, as well as the sedimentological and stratigraphic framework of the study area, the reader can refer to Brigaud et al. (2014) for more details. The diagenetic framework and the petro-geochemical characterization of the samples, including cathodoluminescence (CL) response, fluid inclusion, $\delta^{18}\text{O}$ and $\delta^{13}\text{C}$ are given in Brigaud et al., (2009). Blocky calcite 1 and 2 from Brigaud et al., (2009) are merged here into Calcite 1 (Cal1). Bc3 from Brigaud et al., (2009) is called Cal2 here. Calcite cement Cal1 exhibits a fine (<50 μm) bright orange sub-zone (Cal1a, corresponding to Bc1 in Brigaud et al., 2009) under CL followed by a large (200 μm to few mm) dull brown sub-zone (Cal1b, corresponding to Bc2 in Brigaud et al., 2009). Calcite Cal2, mainly occurring in fractures, consists of dark brown CL spars (corresponding to Bc3 in Brigaud et al., 2009). The isotopic compositions $\delta^{18}\text{O}$ and $\delta^{13}\text{C}$ (and locally $^{87}\text{Sr}/^{86}\text{Sr}$) have been measured in the following samples: bivalves ET7, cement Cal1 in sample E011 (including $^{87}\text{Sr}/^{86}\text{Sr}$), E076B, E115, HTM4 including $^{87}\text{Sr}/^{86}\text{Sr}$, E160 including $^{87}\text{Sr}/^{86}\text{Sr}$. All data are listed in Table S1 (Supplementary data B in Brigaud et al., 2009). Geodic cement in vugs (samples G4 and G8) have been dated by U-Pb isotopic dilution method by Pisapia et al., (2018).

Almost all fluid inclusions observed in blocky calcites are one-phase (liquid) aqueous inclusions. Inclusions are flat and small (< 10 μm) and grouped in fluid inclusions assemblages (FIAs) that do not crosscut the crystal borders, suggesting a primary origin. Very rare two-phase fluid inclusions were observed in one sample: samples E107 crystallizing at 109°C (Fig. S1). These two-phase fluid inclusions in this sample are single, large inclusions located very close to the metastable one-phase FIA. The large volume of the vapor phase in these two-phase inclusions suggests that they were subjected to stretching, and therefore were not considered as representative of the trapping conditions. Other colleagues studied the same cements and never observed two-phase fluid inclusions in these blocky calcite cements, i.e. PhD thesis of Vincent, (2001) and Vincent et al., (2007) for Cal1 of the Oxfordian limestones, Buschaert et al., (2004) for Cal1 and Cal2 within the Bathonian and Oxfordian limestones.

The petrography of the calcites is similar between the three Cal2 samples, crystallizing from 30°C (EST30573) to 90°C (HTM4). All inclusions in Cal2 are small and consist of one-phase fluid inclusions, even for the HTM4 sample crystallizing at 90°C (Fig. S1).

Sample	Carbonate stage	Stratigraphic Stage / Ammonite zone	Sedimentary Formations	Borehole	Depth (m)	CL Response	d ¹³ Ccal ‰, VPDB	d ¹⁸ Ocal ‰, VPDB	87Sr/86Sr
E-T7A1	<i>Trichites</i>	Early Bajocian / humphriesianum	Calcaires à Polypiers	EST210	750	Non-Luminescent	3.10	-1.17	
E-T7A2	<i>Trichites</i>	Early Bajocian / humphriesianum	Calcaires à Polypiers	EST210	750	n. l. bivalves	3.13	-1.01	
E-T7A3	<i>Trichites</i>	Early Bajocian / humphriesianum	Calcaires à Polypiers	EST210	750	n. l. bivalves	2.54	-1.24	
E-T7A4	<i>Trichites</i>	Early Bajocian / humphriesianum	Calcaires à Polypiers	EST210	750	n. l. bivalves	2.54	-0.63	
E-T7A5	<i>Trichites</i>	Early Bajocian / humphriesianum	Calcaires à Polypiers	EST210	750	n. l. bivalves	2.63	-0.81	
E-T7B1	<i>Trichites</i>	Early Bajocian / humphriesianum	Calcaires à Polypiers	EST210	750	n. l. bivalves	3.11	-1.39	
E-T7B2	<i>Trichites</i>	Early Bajocian / humphriesianum	Calcaires à Polypiers	EST210	750	n. l. bivalves	3.08	-1.23	
E-T7B3	<i>Trichites</i>	Early Bajocian / humphriesianum	Calcaires à Polypiers	EST210	750	n. l. bivalves	3.11	-1.24	
E011-1	Cal1	Early Bathonian / zigzag	Calcaires de Chaumont	EST210	584.5	Bright orange	2.73	-5.59	0.707293
E011-2	Cal1	Early Bathonian / zigzag	Calcaires de Chaumont	EST210	584.5	Bright orange	2.66	-6.16	
G8 EST29185	Cal1	Late Bajocian	Marnes de Longwy	EST443	885	Bright orange	2.28	-6.67	
G8 EST29185	Cal1	Late Bajocian	Marnes de Longwy	EST443	885	Bright orange	2.26	-6.80	
G8 EST29185	Cal1	Late Bajocian	Marnes de Longwy	EST443	885	Bright orange	2.25	-6.69	
E076-2	Cal1	Late Bajocian / garantiana	Oolite miliaire inf.	EST210	689.3	Dull brown	1.91	-6.07	
E076B	Cal1	Late Bajocian / garantiana	Oolite miliaire inf.	EST210	689.3	Dull brown	1.65	-7.71	
E076B4	Cal1	Late Bajocian / garantiana	Oolite miliaire inf.	EST210	689.3	Dull brown	1.79	-6.30	
E115	Cal1	Late Bajocian / niortense	Marnes de Longwy	EST210	722.9	Dull brown	0.96	-5.15	
E160-1	Cal1	Early Bajocian / humphriesianum	Calcaires à Polypiers	EST210	763.9	Dull brown	2.49	-6.93	
E160-2	Cal1	Early Bajocian / humphriesianum	Calcaires à Polypiers	EST210	763.9	Dull brown	2.23	-6.50	0.707227
HTM4	Bc2	Late Bathonian / discus	Oolite de Fréville	HTM102	484.5	Dark brown	1.27	-10.13	
HTM5	Cal2	Late Bathonian / discus	Oolite de Fréville	HTM103	484.5	Dark brown	1.83	-9.84	0.707434
HTM6	Cal2	Late Bathonian / discus	Oolite de Fréville	HTM104	484.5	Dark brown	1.52	-9.76	
HTM7	Cal2	Late Bathonian / discus	Oolite de Fréville	HTM105	484.5	Dark brown	1.56	-9.78	
G4 EST07057	Cal2	Middle Oxfordian	Mésangère Fm	EST205	375	Dark brown	2.68	-8.98	
G4 EST07057	Cal2	Middle Oxfordian	Mésangère Fm	EST205	375	Dark brown	2.70	-8.90	

G4 EST07057	Cal2	Middle Oxfordian	Mésangère Fm	EST205	375	Dark brown	2.72	-8.98	
----------------	------	------------------	--------------	--------	-----	------------	------	-------	--

Table S1. Location, CL response and isotopic compositions ($\delta^{18}\text{O}$, $\delta^{13}\text{C}$, and $^{87}\text{Sr}/^{86}\text{Sr}$) previously measured in carbonate samples (Brigaud et al., 2009), and in Pisapia et al., (2018) for samples G4 EST07057 and G8 EST29185.

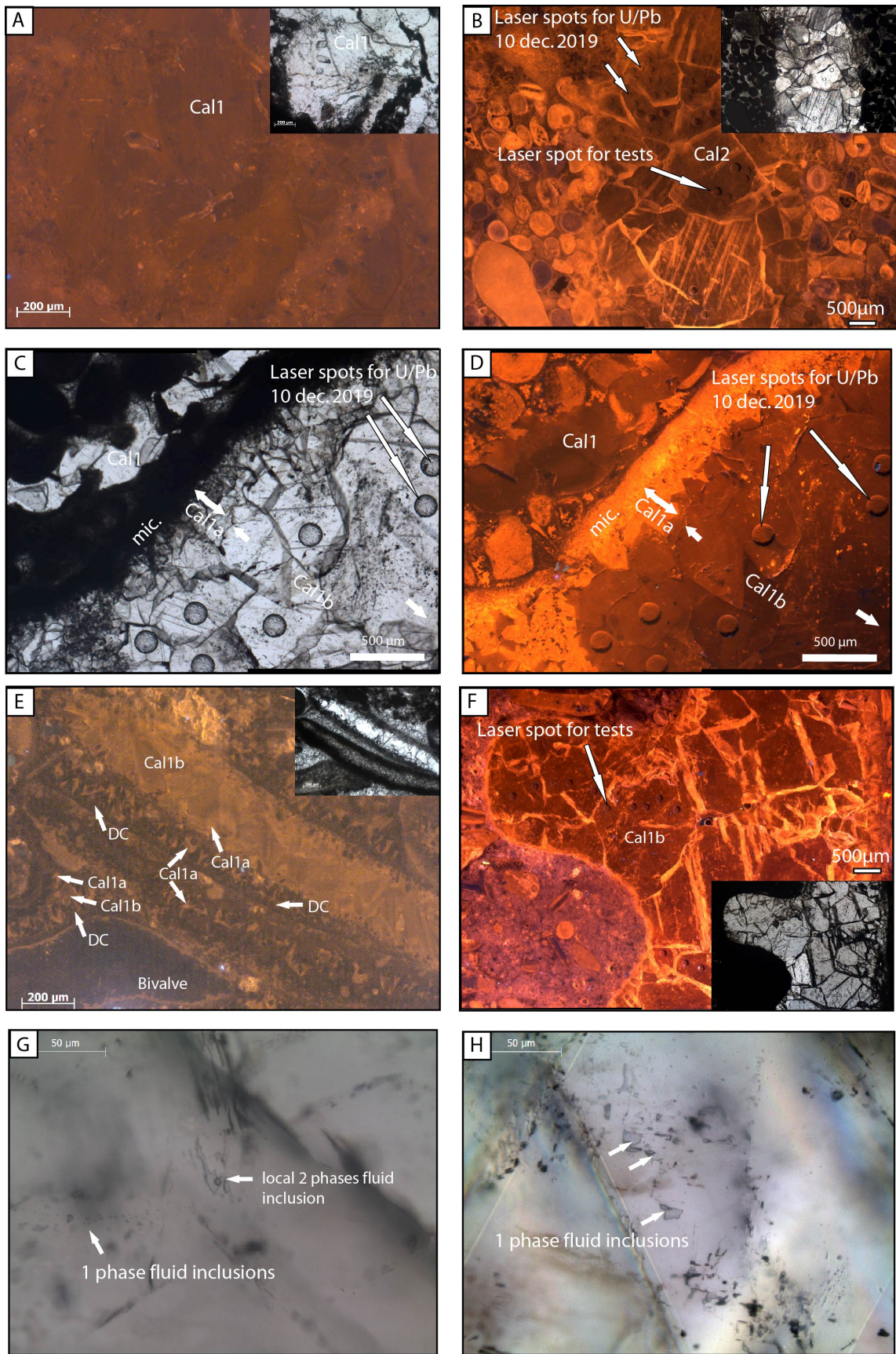


Figure S1. A- Vug in peloidal wackstone displaying Blocky calcite 1 (Cal1), Calcaire de

Chaumont, EST210 core, thin section E011, 584.5 m ($T_{\Delta 47} = 54^{\circ}\text{C}$; Age = 147.7 ± 4.7 Ma). B- Blocky calcite 2 (Cal2) filling fracture in the Oolite de Fréville, HTM102 core, thin section HTM4, 484.5 m ($T_{\Delta 47} = 90^{\circ}\text{C}$; Age = 41.5 ± 4.8 Ma). C- Cementation in ooid grainstone, micritization (mic), Blocky calcite Cal1, subzone a and b, Oolite miliaire inférieure, EST210 core, thin section E076B, 689.3 m ($T_{\Delta 47} = 75^{\circ}\text{C}$; Age = 161 ± 8.6 Ma). D- Same sample in CL. E- Cementation in bioclastic grainstone, Dogtooth Cement (DC), Blocky calcite (Cal1, subzone a and b), Marnes de Longwy, EST210 core, thin section E115, 722.9 m ($T_{\Delta 47} = 75^{\circ}\text{C}$). F- Cementation in bioclastic grainstone, Blocky calcite Cal1 (subzone b) recrystallizing within bivalves shell, Marnes de Longwy, EST210 core, thin section E107, 716.9 m ($T_{\Delta 47} = 109^{\circ}\text{C}$; Age = 157.7 ± 7.7 Ma). G- One phase and local two-phase aqueous fluid inclusions in blocky calcite 1 (Cal1), EST210 core, thin section E107, 716.9 m ($T_{\Delta 47} = 109^{\circ}\text{C}$; Age = 157.7 ± 7.7 Ma). H- Single phase aqueous inclusion in Cal2, HTM102 core, thin section HTM4, 484.5 m ($T_{\Delta 47} = 90^{\circ}\text{C}$; Age = 41.5 ± 4.8 Ma).

Diagenetic, thermal and tectono-sedimentary context

Recent results for the study of fluorite or Pb-Zn mineralization in the Southern Paris Basin (Poitou and Morvan) suggest that hot fluids may have circulated during the Late Jurassic and Early Cretaceous above the basement/sediment unconformity (Cathelineau et al., 2012; Gigoux et al., 2015).

Clumped Δ_{47} measurements

Seven cement samples were analyzed from the limestone sedimentary formations of the Middle Jurassic: six from the first stage of the blocky calcite Cal1 (sample E011 in core EST210, sample G8 EST 29185 in core EST433, samples E076B, E107, E115, E160 from EST210 core), and one from the third blocky calcite stage Cal2, (sample HTM4 from core HTM102). Two samples of the Cal2 stage were analyzed on the Oxfordian Limestones (sample G4 EST07057 in core EST205, and sample EST30573 in core EST433). Finally, an ET7 bivalve sample was also analyzed to test hypothesis of post depositional reequilibration of Δ_{47} signal via solid-state reordering of atoms over geological time and/or micro-sampling. We therefore analyzed 2 different aliquots of the same specimen, one crushed (ET7.1), the other microdrilled using a dental microdrill (ET7.2). The 10 samples whose Δ_{47} values were measured, came from samples already been analyzed in stable isotopes $\delta^{18}\text{O}$ and $\delta^{13}\text{C}$ (Brigaud et al., 2009).

The different stages of cements are composed of blocky calcite, that have been identified on the basis of detailed previous petrographic descriptions (Vincent et al., 2007; Brigaud et al., 2009). A detailed description of the carbonate clumped isotope Δ_{47} methods used at Institut de Physique du Globe de Paris (IPGP) at Université de Paris for both data acquisition and treatment is given in Bonifacie et al., (2017) and is only briefly summarized here.

For each analysis, four steps are necessary:

- (1) about 8 mg of powdered calcite is reacted for 20 min with 104% phosphoric acid at 90 °C. The gases produced over this reaction (CO₂ and H₂O) are continuously transferred to a liquid nitrogen (LN₂) trap.
- (2) After complete digestion (extraction yields of 100.2 ± 2.5%), incondensable gases are pumped away and the trapped CO₂ is cryogenically purified from H₂O by passing through an ethanol-LN₂ trap hold at - 117 ± 6 °C to be eventually collected in a second LN₂ trap.
- (3) Gaseous CO₂ then passes through silver wool and Porapak-Q, 50–80 mesh polymer. Purified CO₂ is then transferred to the Thermo MAT 253 mass spectrometer and analyzed for its Δ_{47} , $\delta^{18}\text{O}$ and $\delta^{13}\text{C}$ compositions. The mass spectrometer is configured to simultaneously measure masses 44 through 49 of the sample CO₂ with respect to a working reference gas provided by Oztech Trading Corporation (with $\delta^{18}\text{O}_{\text{PDB}} = - 6.03\text{‰}$ and $\delta^{13}\text{C}_{\text{PDB}} = - 3.72\text{‰}$ verified through measurements of the international reference material NBS-19). Each measurement consists of seven acquisitions of ten cycles (integration time of 26 s for each cycle) for a total integration time of 1820 s per analysis. Bellows pressure are adjusted to get a signal of 16 V on m/z= 44.
- (4) For constructing correction frames for processing raw Δ_{47} values, CO₂ gases driven to isotopologue equilibrium at both 1000 °C and 25 °C were used. The equilibrated CO₂ gas standards use in this study have bulk isotopic compositions spanning the entire range of measured calcite samples, were purified and analyzed in the same way as calcite samples and standards and were typically run every four to five analyses. The raw Δ_{47} data were first corrected for linearity effects using a fixed common equilibrated gas line EGL slope fitted to the equilibrated CO₂ gases at both 1000 °C and 25 °C. The slope of the EGL over the course of this study was 0.0038 ± 0.0006. Subsequently, the Δ_{47} data were then referenced to the absolute reference frame (or CDES for Carbon Dioxide Equilibrated Scale) of Dennis et al., (2011) using an empirical transfer function (ETF) we built with multiple analyses of the CO₂ gases driven to isotopologue equilibrium at both 1000 °C and 25 °C with theoretically predicted Δ_{47} values of 0.0266‰ and 0.9252‰, respectively (Wang et al., 2004).

As our samples were digested at 90 °C, an acid correction factor of 0.082‰ (Defliese et al., 2015) was added to the Δ_{47} results in order to report the data in a 25 °C acid digestion frame (i.e. $\Delta_{47\text{CDES}25}$). All carbonate samples were analyzed two or three times (using sub-fractions of the same powder) to account for heterogeneity. Also, the samples were analyzed in four discrete sessions of analyses separated by several weeks (that is using ETF correction frames based on various sets of data on CO₂ standards equilibrated at known

temperatures) in order to eliminate possible bias from potential error in constructing the four discrete ETF.

Traditional $\delta^{18}\text{O}$ and $\delta^{13}\text{C}$ data were acquired as part of each Δ_{47} analysis and ^{17}O corrections were made using the ^{17}O parameters from Santrock et al., (1985) as for the large majority of Δ_{47} data and $\Delta_{47} - T$ calibrations published to date. Noticeably, the use of the ^{17}O parameters from Brand et al., (2010) instead, as recently recommended, would only lead here to small differences in Δ_{47} values for both standards and samples (i.e. less than $\pm 0.010\text{‰}$) – that is within the analytical uncertainty for Δ_{47} measurements. This would thus not change significantly neither the reported temperatures nor the conclusions of this study. In order to account for the temperature dependence of oxygen isotope fractionation between CO_2 gas and calcite resulting from the reaction with phosphoric acid at $90\text{ }^\circ\text{C}$ in common acid bath, a fractionation factor of 1.00811 was used (Katz et al., 2017). The $\delta^{13}\text{C}_{\text{cal}}$ and $\delta^{18}\text{O}_{\text{cal}}$ are normalized to NBS19 international standard.

To ensure accuracy of $\Delta_{47\text{CDES}}$ data and the entire data reduction process described above, we routinely analyzed two carbonate reference materials (IPGP-Carrara marble and 102-GCAZ01b, also reported by Dennis et al., 2011 and many other studies) distributed within the unknown samples in all runs. This allows checking for analytical stability/accuracy of the whole procedure (including carbonate digestion, CO_2 purification, stability of the conditions for analyses of CO_2 inside the mass spectrometer and accuracy of the correction frames constructed with standards of equilibrated CO_2 gas – namely the accuracy of the EGL and ETF), as well as long-term reproducibility of the Δ_{47} measurements. The Δ_{47} values obtained for these carbonates over the course of this study (February 2014–May 2015) are: $\Delta_{47} = 0.390 \pm 0.016\text{‰}$ (1 S.D.; n: 16) for IPGP-Carrara; $\Delta_{47} = 0.706 \pm 0.015\text{‰}$ (1 S.D., n: 11) for 102-GC-AZ01b. Those Δ_{47} values are indistinguishable from data obtained in previous studies. Furthermore, the standard deviations of carbonate reference materials reported here on a relatively small number of replicated measurements (n= 16 and n= 12 on the four sessions of analyses, respectively) are consistent with the long-term external reproducibility obtained at IPGP over three years (typically $\pm 0.014\text{‰}$, 1 S.D., n > 200); (Bonifacie et al., 2017).

Finally, the Δ_{47} data were converted into temperatures using the inter-laboratory $\Delta_{47}-T$ calibration recently determined for various types of carbonates with growth temperatures ranging from $-1\text{ }^\circ\text{C}$ to $300\text{ }^\circ\text{C}$ (i.e., Eq. (3) from Bonifacie et al. (2017), $\Delta_{47\text{CDES}25} = 42200/T^2 + 0.2082$ in the $25\text{ }^\circ\text{C}$ acid digestion reference frame). The oxygen isotopic composition of the water from which the calcite precipitated ($\delta^{18}\text{O}_{\text{water}}$) was calculated using the $\delta^{18}\text{O}_{\text{cal}}$ of the carbonate, the temperature estimates of the Δ_{47} data, as well as the value of fractionation equation of oxygen isotopes between calcite and water from Watkins et al., (2013), that is $1000\ln\alpha_{\text{calcite-H}_2\text{O}} = (17,747/T^\circ\text{K}) - 29.777$ for the temperature estimated out of the Δ_{47} data.

Δ_{47} discussion

Because the $T\Delta_{47}$ temperatures we found here were unexpectedly too high (by up to 60°C) compared to the lower temperatures inferred from other geothermometers i.e. fluid inclusions, clay minerals, apatite fission tracks, T_{\max} or vitrinite reflectance (Blaise et al., 2014), we tested the hypothesis that the initial Δ_{47} value acquired at the time of precipitation might have been reset via solid-state reordering of atoms in carbonate lattice during heating over geological time and/or micro-sampling (Passey and Henkes, 2012; Stolper and Eiler, 2015; Lloyd et al., 2018). In the following, we rule out this hypothesis with three lines of reasoning.

First, when injecting the well-known long-term temperature-time path of the studied area (Blaise et al., 2014) into the python software package provided by Lloyd et al. (2018) Figure S2 shows that absolutely no changes in Δ_{47} values of calcites are predicted through solid-state reordering expected for the two models and sets of kinetic parameters existing to date (Passey and Henkes, 2012; Stolper and Eiler, 2015).

Second, Δ_{47} values have been reported for cements of comparable ages in the center of the Paris Basin (Mangenot et al., 2018), in which limestones were buried more deeply and so probably experienced slightly higher temperatures (Espitalie et al., 1987). For those samples, a perfect match was found between $T\Delta_{47}$ and temperatures determined by fluid inclusion microthermometry (Mangenot et al., 2017). As importantly, some of these cements were also directly characterized for their $\delta^{18}\text{O}_{\text{water}}$ in fluid inclusions by cavity ring down spectroscopy (Dassié et al., 2018). The fact that directly measured $\delta^{18}\text{O}_{\text{water}}$ values agree within 1‰ with those calculated from combined $T\Delta_{47}$ and $\delta^{18}\text{O}_{\text{carb}}$ of the host-mineral suggests both isotopic equilibrium at the time of crystallization and that no substantial isotopic change occurred in the host carbonate since then (e.g., via solid-state reordering).

Third, the bivalve sampled from the same level from which two calcite cements display unexpectedly high temperatures (E107 at 109 °C and E115 at 75 °C) yields a $T\Delta_{47}$ of 27 °C and $\delta^{18}\text{O}_{\text{water}}$ of -0.2‰. This is consistent with growth conditions expected during the Jurassic at tropical latitudes (Dera et al., 2011).

Finally, we also investigated the possibility of partial Δ_{47} resetting *via* sampling of the carbonate powder by comparing Δ_{47} obtained after both drilling and crushing of the *Trichites* shell (see Appendix 1). The Δ_{47} data obtained are identical (sample ET7.1 and ET7.2 of 0.676‰), demonstrating that the Δ_{47} is well preserved by the prismatic crystals of the *Trichites* shell.

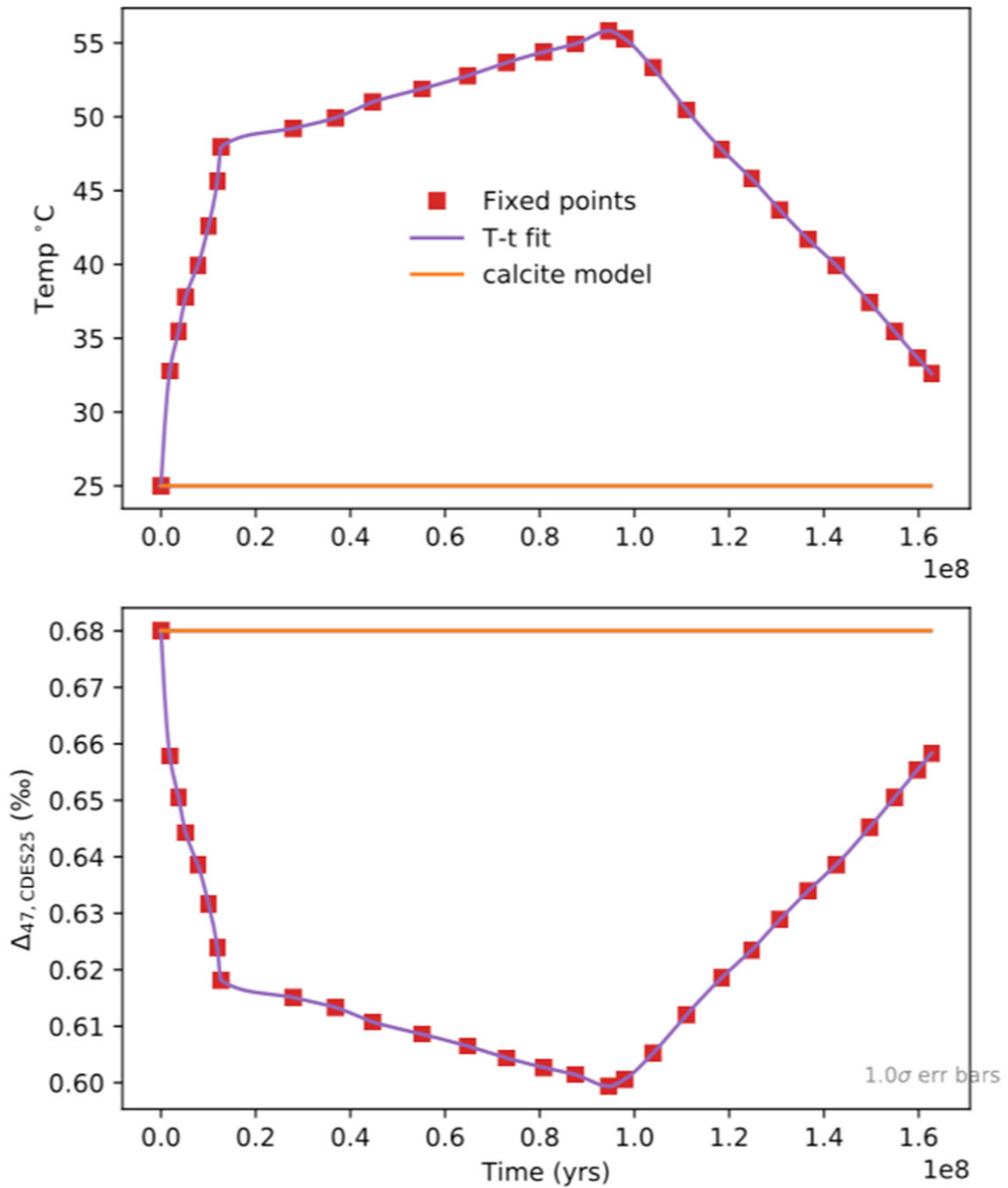


Figure S2. Isothermal heating models of calcite Δ_{47} reordering. Purple line denotes the true temperature-time path of each run. Orange line is calcite Δ_{47} apparent equilibrium temperatures predicted for each run using solid-sate reordering models of both Passey and Henkes (2012) and Stolper and Eiler (2015).

In situ U-Pb ages

Measurements have been made on 4 calcite samples (1) E011 (n = 50), (2) E076B (n = 49), (3) E107 (n = 49) and (4) HTM4 (n = 40) where U and Pb are sufficiently abundant to perform isotopic analyses.

U-Pb laser ablation (LA) analyses were made using a Thermo Scientific™ High Resolution Inductively Coupled Plasma Mass Spectrometer (HR-ICP-MS) ELEMENT XR (ThermoFisher Scientific, Waltham, USA) coupled to a 193 nm Photon Machines (Teledyne, Thousand Oaks, USA) laser at the Géosciences Paris Sud (GEOPS) laboratory at the University Paris-Saclay.

The laser beam diameter for calcite unknowns and calcite reference materials was 150 µm. Calcite crystals (including reference materials) were ablated at a frequency of 8 Hz and a fluence of 1 J.cm⁻², forming a crater 4–5 µm deep. Glass reference materials NIST612 (37.38 ppm U and 38.57 ppm Pb) and NIST614 (0.823 ppm U and 2.32 ppm Pb, Jochum et al., (2011)) were ablated at a frequency of 10 Hz, a fluence of 6.25 J.cm⁻² and a beam size of 40 µm for NIST612 and 110 µm for NIST614.

Each analysis consists of 30 s background acquisition followed by 30 s of sample ablation and 30 s washout. Prior to analysis, each spot was pre-ablated during 7 s at a frequency of 8 Hz and with a fluence of 1 J.cm⁻² over an area larger than the beam diameter to clean the surface (155 µm) and remove potential Pb contamination. The laser-induced aerosol was carried by helium (large volume at 0.5 l.min⁻¹ and inner cup at 0.375 l.min⁻¹) from the sample cell to a mixing funnel in which the sample and He are mixed with 0.950 to 1 l.min⁻¹ argon to stabilize the aerosol input to the plasma. Signal strength of the ICPMS was tuned for the best sensitivity while keeping Th/U between 0.97 and 1.03 and ThO/Th below 0.3 on NIST612. Isotopes ²⁰⁶Pb, ²⁰⁷Pb, ²⁰⁸Pb, ²³²Th and ²³⁸U were acquired with integration time per peak (ms) of 10 ms for ²⁰⁸Pb, ²³²Th, ²³⁸U, of 30 ms for ²⁰⁶Pb and of 40 ms for ²⁰⁷Pb by 70 runs.

We used NIST614 to correct for ²⁰⁷Pb/²⁰⁶Pb fractionation (Woodhead et al., 2016; Roberts et al., 2017). For mass-bias correction of the measured ²³⁸U/²⁰⁶Pb ratios, we used the calcite reference material from the Permian Reef Complex Walnut Creek (WC-1, Roberts et al., 2017). This calcite reference material has been previously dated by thermal ionization mass spectrometry (TIMS) after isotope dilution at 254.4±6.4 Ma and has been used in many other labs for laser ablation mass-bias correction (Li et al., 2014; Coogan et al., 2016; Ring and Gerdes, 2016; Roberts and Walker, 2016; Roberts et al., 2017; Pagel et al., 2018; Lawson et al., 2018; Parrish et al., 2018). WC-1 exhibits high U/Pb and homogeneous distribution of U (Roberts et al., 2017). To ensure accuracy, we analyzed two secondary calcite reference materials during the analytical session: Duff Brown Tank (DBT) calcite, dated at 64.0±0.7 Ma by U-Pb isotope dilution (Hill et al., 2016), and AUG-B6, a calcite breccia dated at 43.0±1.0 Ma (Pagel et al., 2018). Internal secondary reference calcite AUG-B6 comes from the Gondrecourt graben (Eastern Paris Basin), part of the European Cenozoic Rift System, and has been dated by Pagel et al. (2018) by LA-ICPMS, and is routinely analyzed at GEOPS

(university Paris-Saclay). Measurements have been made by sequences composed of 6 reference material analyses (2 NIST612, 2 NIST614 and 2 WC-1), 10 spots on unknowns calcite, 8 reference material analysis (2 NIST614, 2 WC-1, 2 DBT and 2 AUG-B6), 10 spots on unknowns calcite, etc., ending with 6 reference material analysis (2 NIST612, 2 NIST614 and 2 WC-1). Data were acquired in fully automated mode overnight in a sequence of 336 analyses for about 12 hours of analysis the 10-11 December 2019.

Data were reduced in *Iolite*© using NIST614 glass as the primary reference material to correct for baseline and for Pb isotope mass bias over the sequence time (Paton et al., 2011; Lawson et al., 2018). No down-hole fractionation correction is applied in *Iolite*© (Nuriel et al., 2017). The traditional approach to data reduction was to define an acceptable and large window (time window of >25 s if possible) within the data profile and average the ratios. Calcite typically has low (< 2-3 ppm) to very low (< 1 ppm) U concentration. The most favorable samples for dating are those with highest U/Pb and lowest $^{207}\text{Pb}/^{206}\text{Pb}$ values, *i.e.* with very low initial common Pb (Lawson et al., 2018; Parrish et al., 2018). The two sigma error in $^{207}\text{Pb}/^{206}\text{Pb}$ and $^{206}\text{Pb}/^{238}\text{U}$ ratios measured on NIST614 during the analytical session were propagated to the final age uncertainty of calcite samples by quadratic addition. During the session, NIST614 two sigma error of the $^{207}\text{Pb}/^{206}\text{Pb}$ was 0.22 % and was 0.76 % for $^{206}\text{Pb}/^{238}\text{U}$. Signal peak of ^{206}Pb , ^{207}Pb or ^{238}U can sometimes occur, causing anomalously high $^{206}\text{Pb}/^{238}\text{U}$ or $^{207}\text{Pb}/^{206}\text{Pb}$ standard error (2σ), typically greater than 30 %. Twelve anomalous spots (10 on E011, 1 on E107 and 1 on HTM4) were excluded due to large peak in ^{207}Pb . Each reduced data is plotted in a $^{238}\text{U}/^{206}\text{Pb}$ versus $^{207}\text{Pb}/^{206}\text{Pb}$ graph using *Isoplot* (inverse concordia isochron in *Isoplot* (Ludwig, 2012)). An isochron is drawn and the isochron age is deduced by the intersection on the concordia. For each sequence, the age and uncertainty of WC-1 reference calcite, following normalization using NIST614 glass, was calculated without further normalization using a Tera-Wasserburg intercept age calculated from the NIST614-normalized $^{206}\text{Pb}/^{238}\text{U}$ and $^{207}\text{Pb}/^{206}\text{Pb}$ ratios. Following the analytic run, we applied a linear correction factor to correct the $^{206}\text{Pb}/^{238}\text{U}$ such that the primary WC-1 yields the correct intercept age (*i.e.*, 254.4 ± 6.4 Ma, Roberts et al., 2017). Throughout the analytical session (Fig. S3), we obtained 175.7 ± 2.3 Ma for WC1 (36 analyses), hence we applied a linear correction factor of 0.685 to correct all the $^{206}\text{Pb}/^{238}\text{U}$ ratios of carbonate samples. We anchored the $^{207}\text{Pb}/^{206}\text{Pb}$ ratio at 0.85 for the common Pb based on Stacey and Kramers (1975) when we calculated the Tera-Wasserburg intercept age on WC-1 (see Roberts et al., 2017). On unknown calcite samples, Tera-Wasserburg intercept ages are calculated by plotting each spots from a single sample (or a single calcite type) and by applying the linear correction factor (0.685) found on WC-1 during the session to correct the $^{206}\text{Pb}/^{238}\text{U}$. An age is calculated from the *Isoplot*© software without any constraint on the initial $^{207}\text{Pb}/^{206}\text{Pb}$ value. Error ellipses of each spots and the error on the Tera-Wasserburg intercept age are 2σ . For each Tera-Wasserburg Concordia diagram, two estimates of age

uncertainty have been calculated by propagating uncertainties through quadratic addition. The first one accounts for uncertainties on ^{235}U and ^{238}U decay constants ($\pm 6.7 \times 10^{-7} \text{ Mys}^{-1}$ for $\lambda_f^{235}\text{U}$ and $\pm 8.3 \times 10^{-8} \text{ Mys}^{-1}$ for $\lambda_f^{238}\text{U}$, Fig. 2 and Fig. S3), while the second one accounts for uncertainties on decay constants, primary reference material WC-1 age (2.6 %), and the two sigma error on $^{207}\text{Pb}/^{206}\text{Pb}$ (0.22 %) and $^{206}\text{Pb}/^{238}\text{U}$ (0.76 %) ratios of the analytical session. Following this description, calculated ages for secondary reference materials analyzed during the sequence were $43.4 \pm 1.5 \text{ Ma}$ for AUG-B6 (MSWD = 1.7) and $66.7 \pm 4.6 \text{ Ma}$ for DBT (MSWD = 3.1), without anchoring $^{207}\text{Pb}/^{206}\text{Pb}$ at the origin. These ages are identical within analytical uncertainty to the ages published for these two calcites (Fig. S3, Pagel et al., 2018, Hill et al., 2016, respectively).

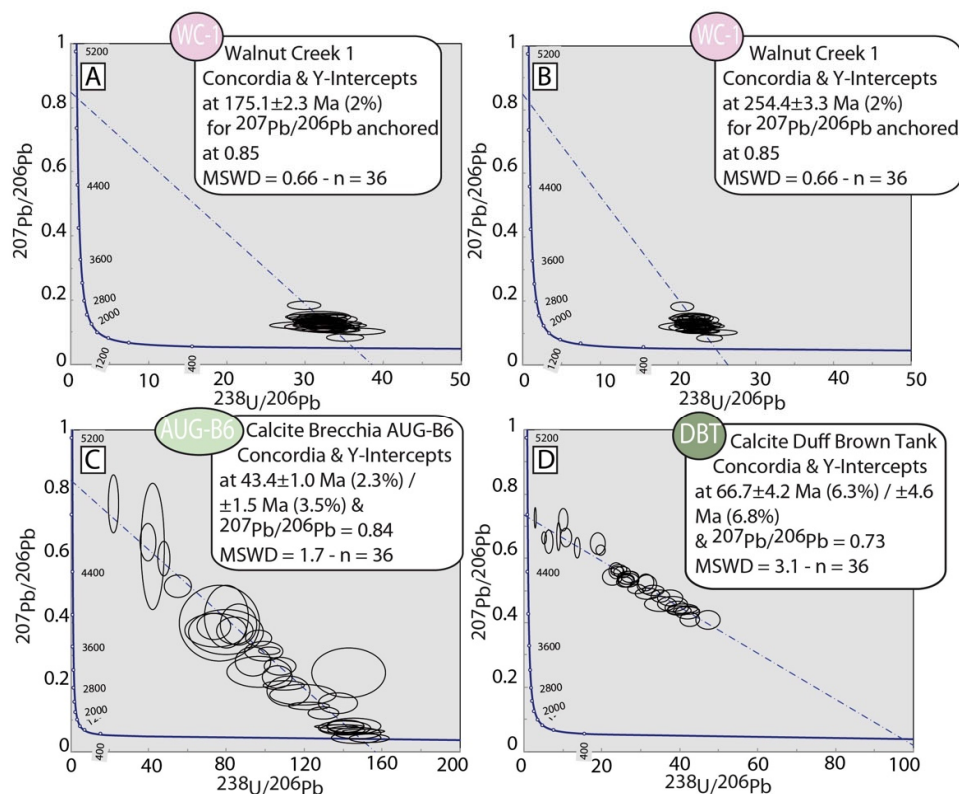


Figure S3: A- Tera-Wasserburg diagrams of the Permian Reef Complex Walnut Creek (WC-1, Roberts et al., 2017) calcite reference material analysis during the session displaying uncorrected age at $175.1 \pm 2.3 \text{ Ma}$. WC-1 is dated by thermal ionization mass spectrometry (TIMS) after isotope dilution at $254.4 \pm 6.4 \text{ Ma}$. B- Age of WC-1 after applying a linear correction factor of 0.685 to correct the $^{238}\text{U}/^{206}\text{Pb}$ ratios. C- Tera-Wasserburg diagrams displaying an age of $43.4 \pm 1.5 \text{ Ma}$ for the in-house calcite Breccia of the Gondrecourt graben measured during the analytical session (AUG-B6, Pagel et al., 2018). D- Tera-Wasserburg diagram displaying the Duff Brown Tank at $66.7 \pm 4.6 \text{ Ma}$ measured during the analytical session (Isotope dilution age at $64 \pm 0.7 \text{ Ma}$, Hill et al., 2016).

Laboratory and Sample Preparation	
Laboratory name	Géosciences Paris Sud (GEOPS), University Paris-Saclay, Orsay, France
Sample type/mineral	Calcite
Sample preparation	Polished thin section 30 µm
Imaging	Cathodoluminescence microscope
Laser ablation system	
Make, Model and type	193nm ArF Photon Machines (Teledyne)
Ablation cell	HelEx
Laser wavelength (nm)	193 m
Pulse width (ns)	5 ns
Fluence (J.cm ⁻²)	1 J.cm ⁻²
Repetition rate (Hz)	8 Hz
Pre-ablation	each spot during 7 s, 155 µm
Ablation duration (secs)	30 s
Spot size (mm)	150 µm
Sampling mode / pattern	Static spot ablation
Carrier gas	He
Cell carrier gas flow (l.min ⁻¹)	Helium Lage volume: 0.5 l.min ⁻¹ Inner cup: 0.375 l.min ⁻¹
ICPMS instrument	
ICPMS instrument Make, Model & type	ThermoScientific Element XR
Sample introduction	Ablation aerosol
RF power (W)	1175 W
Make-up gas flow in ablation funnel (l.min ⁻¹)	Ar=0.950 to 1 l.min ⁻¹
Detection system	Ion counter
Masses measured	206, 207, 208, 232, 238
Average gas background (cps)	30 for 206, 27 for 207, 67 for 208, 0.1 for 232, 0 for 238
Integration time per peak (ms)	30 ms for 206, 40 ms for 207, 10 ms for 208, 10 ms for 232, 10 ms for 238

Total integration time per reading (secs)	0.1 s
JC Dead time (ns)	30 ns
Signal strength at ICPMS tuned conditions	Th/U=1 248ThO/232Th below 0.3
Data Processing	
Data acquisition	Fully automated mode overnight in sequences of 399 analysis maximum
Gas blank	30 s background, 30 s sample ablation and 30 s washout
.Calibration strategy	NIST614 for Pb-Pb, calcite WC-1 for U-Pb, secondary reference material calcite Duff Brown Tank and calcite breccia AUG-B6
Reference Material info	WC-1 age: 254.4±6.4 Ma (Roberts et al., 2017), Duff Brown Tank age: 64±0.7 Ma (Hill et al., 2016) and calcite breccia AUG-B6 age: 43±1 Ma (Pagel et al., 2018)
Data processing package used / Correction for LIEF	lomite to calculate uncertainties, no down-hole fractionation correction
Mass discrimination	$^{207}\text{Pb}/^{206}\text{Pb}$ normalization to NIST614, $^{206}\text{Pb}/^{238}\text{U}$ normalized to WC-1
Common-Pb correction, composition and uncertainty	No common-Pb correction applied
Uncertainty level & propagation	Ages in the data table are quoted at 2sigma (2σ) absolute, uncertainty propagation by quadratic addition
Quality control / Validation	Measurements of WC-1, Duff Brown Tank (DBT) age = 66.7 ± 4.6 Ma, AUG-B6 age = 43.4± 1.5 Ma and NIST614 were done along with samples throughout the analytical session

Table S2: Metadata for LA-ICPMS U-Pb ages of calcite at University Paris-Saclay, GEOPS laboratory.

References

Blaise, T. et al., 2014, Reconstruction of low temperature (<100 °C) burial in sedimentary basins: A comparison of geothermometer in the intracontinental Paris Basin: *Marine and Petroleum Geology*, v. 53, p. 71–87, doi:10.1016/j.marpetgeo.2013.08.019.

Bonifacie, M. et al., 2017, Calibration of the dolomite clumped isotope thermometer from 25 to 350 °C, and implications for a universal calibration for all (Ca, Mg, Fe)CO₃ carbonates: *Geochimica et Cosmochimica Acta*, v. 200, p. 255–279, doi:10.1016/j.gca.2016.11.028.

Brand, W.A., Assonov, S.S., and Coplen, T.B., 2010, Correction for the ¹⁷O interference in δ(¹³C) measurements when analyzing CO₂ with stable isotope mass spectrometry (IUPAC Technical Report): *Pure and Applied Chemistry*, v. 82, p. 1719–1733, doi:10.1351/PAC-REP-09-01-05.

Brigaud, B., Durllet, C., Deconinck, J.-F., Vincent, B., Thierry, J., and Trouiller, A., 2009, The origin and timing of multiphase cementation in carbonates: Impact of regional scale geodynamic events on the Middle Jurassic Limestones diagenesis (Paris Basin, France): *Sedimentary Geology*, v. 222, p. 161–180.

Buschaert, S., Fourcade, S., Cathelineau, M., Deloule, E., Martineau, F., Ayt Ougougdal, M., and Trouiller, A., 2004, Widespread cementation induced by inflow of continental water in the eastern part of the Paris basin: O and C isotopic study of carbonate cements: *Applied Geochemistry*, v. 19, p. 1201–1215, doi:10.1016/j.apgeochem.2003.01.001.

Cathelineau, M., Boiron, M.-C., Fourcade, S., Ruffet, G., Clauer, N., Belcourt, O., Coulibaly, Y., Banks, D.A., and Guillocheau, F., 2012, A major Late Jurassic fluid event at the basin/basement unconformity in western France: ⁴⁰Ar/³⁹Ar and K–Ar dating, fluid chemistry, and related geodynamic context: *Chemical Geology*, v. 322–323, p. 99–120, doi:10.1016/j.chemgeo.2012.06.008.

Coogan, L.A., Parrish, R.R., and Roberts, N.M.W., 2016, Early hydrothermal carbon uptake by the upper oceanic crust: Insight from in situ U–Pb dating: *Geology*, v. 44, p. 147–150, doi:10.1130/G37212.1.

Dassié, E.P. et al., 2018, A Newly Designed Analytical Line to Examine Fluid Inclusion Isotopic Compositions in a Variety of Carbonate Samples: *Geochemistry, Geophysics, Geosystems*, v. 19, p. 1107–1122, doi:10.1002/2017GC007289.

Defliese, W.F., Hren, M.T., and Lohmann, K.C., 2015, Compositional and temperature effects of phosphoric acid fractionation on Δ⁴⁷ analysis and implications for discrepant calibrations: *Chemical Geology*, v. 396, p. 51–60, doi:https://doi.org/10.1016/j.chemgeo.2014.12.018.

Dennis, K.J., Affek, H.P., Passey, B.H., Schrag, D.P., and Eiler, J.M., 2011, Defining an absolute reference frame for ‘clumped’ isotope studies of CO₂: *Geochimica Et Cosmochimica Acta*, v. 75, p. 7117–7131, doi:https://doi.org/10.1016/j.gca.2011.09.025.

Dera, G., Neige, P., Dommergues, J.L., and Brayard, A., 2011, Ammonite paleobiogeography during the Pliensbachian-Toarcian crisis (Early Jurassic) reflecting paleoclimate, eustasy, and extinctions: *Global and Planetary Change*, v. 78, p. 92–105, doi:10.1016/j.gloplacha.2011.05.009.

Espitalie, J., Maxwell, J.R., Chenet, Y., and Marquis, F., 1987, Aspects of hydrocarbon migration in the Mesozoic in the Paris Basin as deduced from an organic geochemical survey: *Organic Geochemistry*, v. 13, p. 467–481.

Gigoux, M., Delpéch, G., Guerrot, C., Pagel, M., Augé, T., Négrel, P., and Brigaud, B., 2015, Evidence for an Early Cretaceous mineralizing event above the basement/sediment unconformity in the intracratonic Paris Basin: paragenetic sequence and Sm-Nd dating of the world-class Pierre-Perthuis stratabound fluorite deposit: *Mineralium Deposita*, v. 50, p. 455–463.

Hill, C.A., Polyak, V.J., Asmerom, Y., and P. Provencio, P., 2016, Constraints on a Late Cretaceous uplift, denudation, and incision of the Grand Canyon region, southwestern Colorado Plateau, USA, from U-Pb dating of lacustrine limestone: U-Pb age of lacustrine limestone: *Tectonics*, v. 35, p. 896–906, doi:10.1002/2016TC004166.

Jochum, K.P. et al., 2011, Determination of Reference Values for NIST SRM 610-617 Glasses Following ISO Guidelines: *Geostandards and Geoanalytical Research*, v. 35, p. 397–429, doi:10.1111/j.1751-908X.2011.00120.x.

Katz, A., Bonifacie, M., Hermoso, M., Cartigny, P., and Calmels, D., 2017, Laboratory-grown coccoliths exhibit no vital effect in clumped isotope ($\Delta 47$) composition on a range of geologically relevant temperatures: *Geochimica Et Cosmochimica Acta*, v. 208, p. 335–353, doi:https://doi.org/10.1016/j.gca.2017.02.025.

Lawson, M. et al., 2018, Deciphering the diagenetic history of the El Abra Formation of eastern Mexico using reordered clumped isotope temperatures and U-Pb dating: *GSA Bulletin*, v. 130, p. 617–629, doi:10.1130/B31656.1.

Li, Q., Parrish, R.R., Horstwood, M.S.A., and McArthur, J.M., 2014, U-Pb dating of cements in Mesozoic ammonites: *Chemical Geology*, v. 376, p. 76–83, doi:10.1016/j.chemgeo.2014.03.020.

Lloyd, M.K., Ryb, U., and Eiler, J.M., 2018, Experimental calibration of clumped isotope reordering in dolomite: *Geochimica et Cosmochimica Acta*, v. 242, p. 1–20, doi:10.1016/j.gca.2018.08.036.

Ludwig, K.R., 2012, User's Manual for Isoplot 7.75 A Geochronological Toolkit for Microsoft Excel: Berkeley Geochronology Center Special Publication, 75 p.

Mangenot, X., Bonifacie, M., Gasparrini, M., Götz, A., Chaduteau, C., Ader, M., and Rouchon, V., 2017, Coupling $\Delta 47$ and fluid inclusion thermometry on carbonate cements to precisely reconstruct the temperature, salinity and $\delta^{18}\text{O}$ of paleo-groundwater in

sedimentary basins: *Chemical Geology*, v. 472, p. 44–57, doi:10.1016/j.chemgeo.2017.10.011.

Mangenot, X., Gasparrini, M., Rouchon, V., and Bonifacie, M., 2018, Basin-scale thermal and fluid flow histories revealed by carbonate clumped isotopes (Δ_{47}) - Middle Jurassic carbonates of the Paris Basin depocentre: *Sedimentology*, v. 65, p. 123–150, doi:10.1111/sed.12427.

Nuriel, P., Weinberger, R., Kylander-Clark, A.R.C., Hacker, B.R., and Craddock, J.P., 2017, The onset of the Dead Sea transform based on calcite age-strain analyses: *Geology*, v. 45, p. 587–590, doi:10.1130/G38903.1.

Pagel, M. et al., 2018, Improving paleohydrological and diagenetic reconstructions in calcite veins and breccia of a sedimentary basin by combining Δ_{47} temperature, $\delta^{18}\text{O}_{\text{water}}$ and U-Pb age: *Chemical Geology*, v. 481, p. 1–17, doi:10.1016/j.chemgeo.2017.12.026.

Parrish, R.R., Parrish, C.M., and Lasalle, S., 2018, Vein calcite dating reveals Pyrenean orogen as cause of Paleogene deformation in southern England: *Journal of the Geological Society*, v. 175, p. 425–442, doi:10.1144/jgs2017-107.

Passey, B.H., and Henkes, G.A., 2012, Carbonate clumped isotope bond reordering and geospeedometry: *Earth and Planetary Science Letters*, v. 351–352, p. 223–236, doi:https://doi.org/10.1016/j.epsl.2012.07.021.

Paton, C., Hellstrom, J., Paul, B., Woodhead, J., and Hergt, J., 2011, Lolite: Freeware for the visualisation and processing of mass spectrometric data: *Journal of Analytical Atomic Spectrometry*, v. 26, p. 2508, doi:10.1039/c1ja10172b.

Pisapia, C., Deschamps, P., Battani, A., Buschaert, S., Guihou, A., Hamelin, B., and Brulhet, J., 2018, U/Pb dating of geodic calcite: new insights on Western Europe major tectonic events and associated diagenetic fluids: *Journal of the Geological Society*, v. 175, p. 60–70, doi:10.1144/jgs2017-067.

Ring, U., and Gerdes, A., 2016, Kinematics of the Alpenrhein-Bodensee graben system in the Central Alps: Oligocene/Miocene transtension due to formation of the Western Alps arc: *Alpenrhein-Bodensee Graben System: Tectonics*, v. 35, p. 1367–1391, doi:10.1002/2015TC004085.

Roberts, N.M.W., Rasbury, E.T., Parrish, R.R., Smith, C.J., Horstwood, M.S.A., and Condon, D.J., 2017, A calcite reference material for LA-ICP-MS U-Pb geochronology: *Geochemistry, Geophysics, Geosystems*, v. 18, p. 2807–2814, doi:10.1002/2016GC006784.

Roberts, N.M.W., and Walker, R.J., 2016, U-Pb geochronology of calcite-mineralized faults: Absolute timing of rift-related fault events on the northeast Atlantic margin: *Geology*, v. 44, p. 531–534, doi:10.1130/G37868.1.

Santrock, J., Studley, S.A., and Hayes, J.M., 1985, Isotopic analyses based on the mass spectra of carbon dioxide: *Analytical Chemistry*, v. 57, p. 1444–1448, doi:10.1021/ac00284a060.

Stacey, J.S., and Kramers, J.D., 1975, Approximation of terrestrial lead isotope evolution by a two-stage model: *Earth and Planetary Science Letters*, v. 26, p. 207–221, doi:https://doi.org/10.1016/0012-821X(75)90088-6.

Stolper, D.A., and Eiler, J.M., 2015, The kinetics of solid-state isotope-exchange reactions for clumped isotopes: A study of inorganic calcites and apatites from natural and experimental samples: *American Journal of Science*, v. 315, p. 363–411.

Vincent, B., 2001, *Sédimentologie et Géochimie de la Diagenèse des carbonates. Application au Malm de la bordure Est du Bassin de Paris* [PhD Thesis]: University of Burgundy, 380 p.

Vincent, B., Emmanuel, L., Houel, P., and Loreau, J.-P., 2007, Geodynamic control on carbonate diagenesis: Petrographic and isotopic investigation of the Upper Jurassic formations of the Paris Basin (France): *Sedimentary Geology*, v. 197, p. 267–289, doi:10.1016/j.sedgeo.2006.10.008.

Wang, Z., Schauble, E.A., and Eiler, J.M., 2004, Equilibrium thermodynamics of multiply substituted isotopologues of molecular gases: *Geochimica Et Cosmochimica Acta*, v. 68, p. 4779–4797, doi:https://doi.org/10.1016/j.gca.2004.05.039.

Watkins, J.M., Nielsen, L.C., Ryerson, F.J., and DePaolo, D.J., 2013, The influence of kinetics on the oxygen isotope composition of calcium carbonate: *Earth and Planetary Science Letters*, v. 375, p. 349–360, doi:10.1016/j.epsl.2013.05.054.

Woodhead, J.D., Horstwood, M.S.A., and Cottle, J.M., 2016, Advances in Isotope Ratio Determination by LA-ICP-MS: *Elements*, v. 12, p. 317–322, doi:10.2113/gselements.12.5.317.